SPT analysis of hydrogen embrittlement in CrMoV welds

G. Álvarez[1*], A. Zafra[1], C. Rodríguez[1,2], F.J. Belzunce[1,2], I.I. Cuesta[2]

[1] SIMUMECAMAT Research Group, Universidad de Oviedo, Edificio Departamental Oeste, 7.1.10. Campus Universitario, 33203 Gijón, Asturias.

[2] Structural Integrity Group, Universidad de Burgos, Escuela Politécnica Superior, Avd. Cantabria s/n, 09006 Burgos, Spain.

*Contact email: alvarezdguillermo@uniovi.es

Abstract

In this paper Small Punch Tests (SPT) are used to determine the mechanical properties of the heat affected zone (HAZ) of CrMoV welded joints and to evaluate the embrittlement caused by the presence of internal hydrogen. Hydrogen permeation tests were carried out to determine the effective diffusion coefficients of the different regions of welded joints, whose hydrogen contents were measured using a hydrogen analyser.

The paper demonstrates that SPTs can be used to estimate the tensile properties and the toughness of small areas, such as the subzones of a welded joint which are not thick enough for machining standard specimens. In cases where it is not possible to determine the fracture toughness of brittle regions using standard SPT samples, tests using longitudinally notched SPT samples were conducted. The normalized energy at failure, W/t^2, was selected as the most appropriate SPT parameter to estimate the fracture toughness regardless of the fracture behaviour of the material (ductile or brittle). It was seen that the fracture toughness of the fine grained HAZ (FG-HAZ) is similar to that of the Base Metal (BM), while the fracture toughness of the coarse grained HAZ (CG-HAZ) is more similar to that of the Weld Metal (WM). The effect of hydrogen on BM and FG-HAZ is low, with embrittlement indexes of about 20%. However, a strong effect of hydrogen was observed in CG-HAZs and WMs, with embrittlement indexes of 60-80%. and a clear change from ductile to brittle behaviour in their fracture surfaces.

1 Introduction

For decades attempts have been made improve the mechanical properties of materials and in particular to obtain the strength necessary to bear the stresses to which they are exposed. In the case of structural steels, the design of welded joints is especially important as they are usually the weakest part of the structure and the most prone to embrittlement. However, the optimization of the mechanical properties of welds is complex. Firstly because welded joints are composed of different subzones with different microstructures and mechanical properties. Secondly because the small size of all these subzones makes machining homogeneous specimens to characterize them with mechanical tests impossible. To overcome this, miniature tests have been developed.

There many types of miniature tests, but the Small Punch Test (SPT) is one of the most common and practical for metallic materials. The advantage of this test is its capacity to estimate the main tensile properties of metallic materials [1–4], and to determine them in aggressive environments [5–8], using small specimens (usually, 10x10x0.5 mm). The standard version of this test, which employs specimens without notch, can also provide the fracture toughness of ductile materials [9]. In order to obtain fracture properties, many researchers recommend the use of notched samples [10–14]. Different types of notched specimens have been proposed, although none of them has yet become established as the optimal one.

Hydrogen embrittlement is a well-known phenomenon which degrades the mechanical properties of metallic components [15–21]. Hydrogen enters steel structures, such as pipes, vessels or off-shore constructions, during different stages of manufacturing (pickling, electro-coating, welding, etc.). Hydrogen can also enter steel from the environment through general and localised corrosion, contact with specific fluids and gases, etc... Most large steel structures have welded joints, in which the weld metal or the coarse grain heat affected zone (CG-HAZ) usually have the greatest hardness and the lowest toughness. In these areas the embrittlement phenomenon is often very evident. Furthermore, the likelihood of defects such as pores, cracks and fusion faults at these locations is also greater. Therefore, the study of the mechanical behaviour of welds is particularly important when the welded structure is affected by internal hydrogen. Failure

of these metallic components usually takes place along the welded zone, as hydrogen embrittlement can produce a serious reduction of their mechanical properties [22].

CrMoV steels are the most widely used steel family in the fabrication of structures subjected to in-service hydrogen environments. The aim of this work is to use SPT to determine the tensile and fracture properties and to analyse the embrittlement caused by internal hydrogen in the different zones of a CrMoV steel welded joint [23,24] .

The subzones of the HAZ were precisely analysed using standard SPT specimens. The results of the Base (BM) and Weld Metal (WM) were compared with the tensile and fracture tests in order to validate them. Once the SPT properties of the homogeneous parts of the weld had been validated, the mechanical properties of the fine and coarse grain zones of the HAZ (FG-HAZ and CG-HAZ respectively) could be estimated. As the presence of a stress concentrator increases hydrogen embrittlement, notched SPT samples extracted from the different zones of the weld were also employed. An analysis of the fracture behaviour of specimens free of hydrogen or with pre-charged hydrogen, makes it possible to determine the influence of internal hydrogen on the fracture behaviour of the welded joint.

2 Materials and mechanical properties

2.1 Materials

The base material (BM) used in this study was a CrMoV steel (SA 542 Grade-D-Class4) received as a 108 mm thick plate. It was normalized at 925ºC for 30 min, quenched in water and tempered at 720ºC for 3 h.

Submerged-arc welding (SAW) with DC current with a heat input of 2.2 kJ/mm (29-32 V, 425-550 A and 45-55 cm/min) and a Thyssen Union S1 CrMo2V electrode were used for the welding process. The minimum and maximum preheating temperatures were 205ºC and 250ºC respectively. Once welded, the coupons were subjected to a dehydrogenation treatment at 350ºC for 4 hours. The chemical compositions of the base (BM) and weld (WM) metals are shown in Table 1.

Table 1. Chemical composition of base and filler metals (% weight)

Material	*C*	*Si*	*Mn*	*Cr*	*Mo*	*V*	*Ni*
WM	0.08	0.04	1.08	2.28	0.93	0.24	0.03

BM	0.15	0.09	0.52	2.27	1.06	0.31	0.19

Figure 1 shows the microstructure of the welded joint. The weld metal (WM) and the heat affected zone (HAZ) are composed of a mixture of martensite and bainite microstructures, while the base metal (BM) has a similar but tempered microstructure. The low temperature dehydrogenation treatment barely modifies the as-welded microstructure. Significant differences can also be seen in the HAZ. Figure 1.b shows a coarser grain size produced in the region located near the fusion line, this is known as the CG-HAZ. Figure 1.c shows the microstructure with a much finer grain size located just near the base metal, the FG-HAZ.

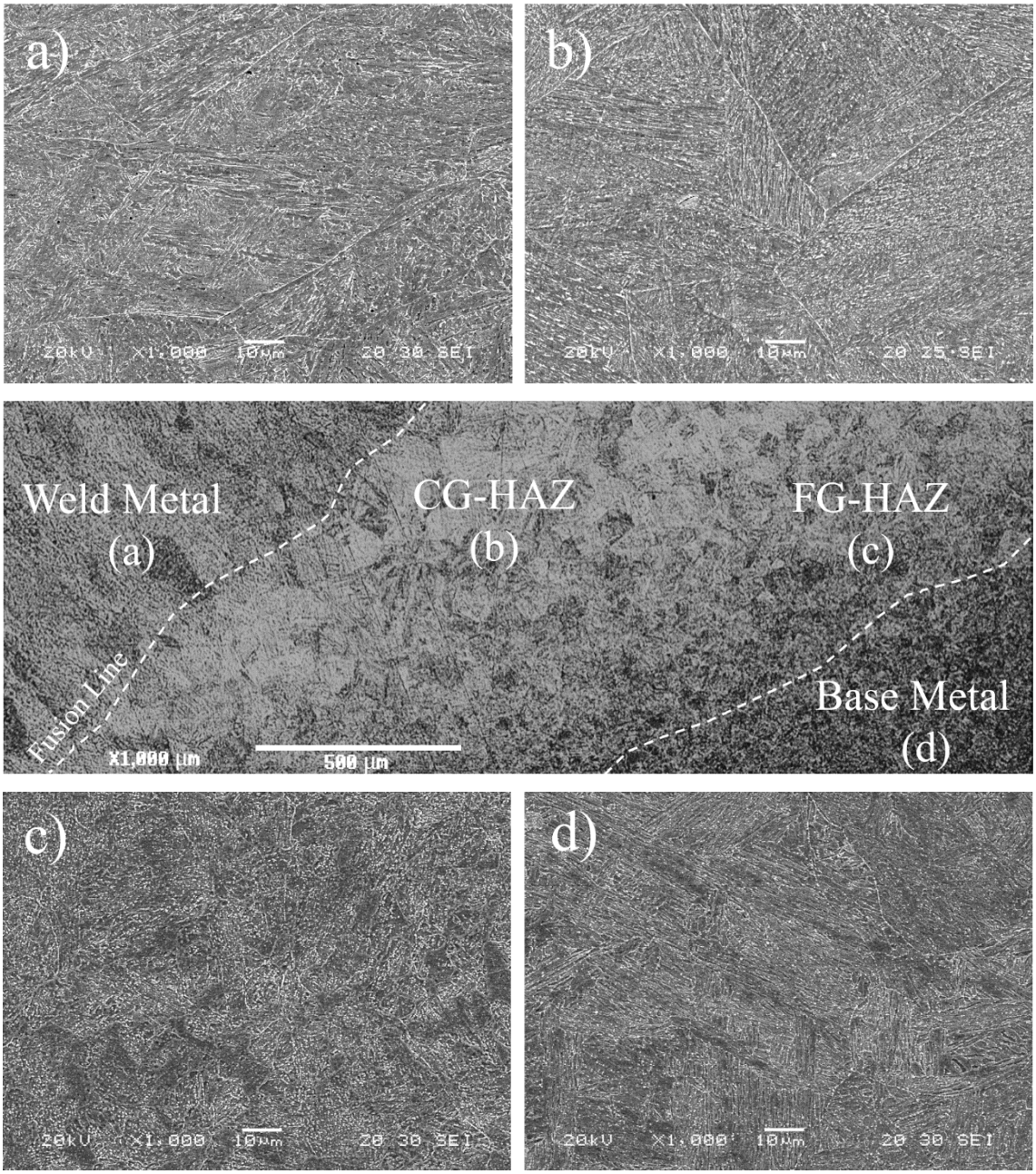

Figure 1. Microstructure of the weld a) weld metal; b) CG-HAZ; c) FG-HAZ; d) base metal

Vickers hardness tests using a 1 kg load were carried out along a horizontal line crossing the joint from BM to WM. Twenty-four indentations were made, four in the BM, nine in the FG-HAZ (the tempered sub-zone is also included in this region), eight in the CG-HAZ and three in the WM. The hardness results are shown in Figure 2, where the recorded HV1 hardness is plotted against the distance from the fusion line. As can be seen, the CG-HAZ has the greatest hardness values, followed closely by the WM. There is a clear decline of hardness from the fine-grained zone (FG-HAZ) to the BM, with the lowest hardness corresponding to the over-tempered microstructure, located adjacent to the BM. Table 2 shows the hardness mean values and the coefficients of variation for the four aforementioned weld subzones.

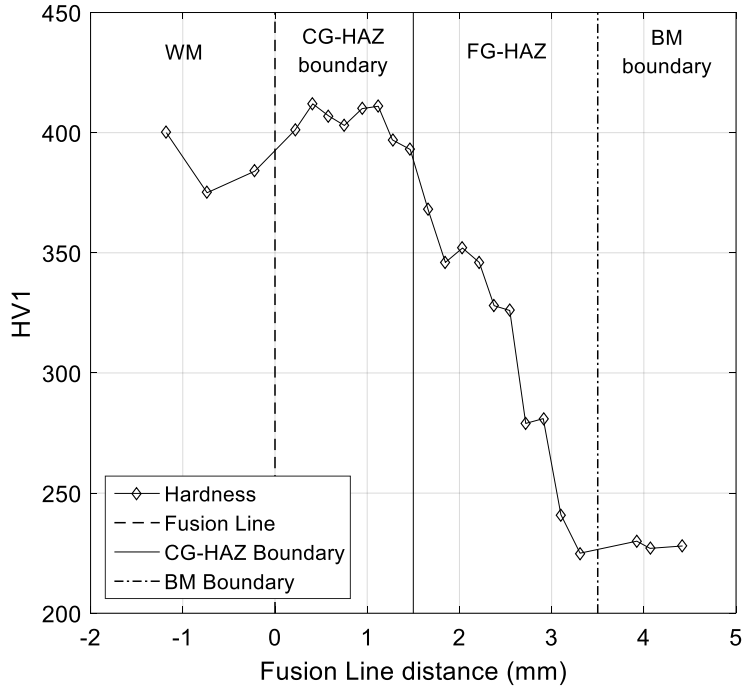

Figure. 2. Hardness evolution along the welded joint

Table 2. Hardness results (mean ± Coeff. of variation, %)

Hardness	*WM*	*CG-HAZ*	*FG-HAZ*	*BM*
HV1	386 ± 3	405 ± 2	332 ± 15	228 ± 1

2.2 Mechanical characterization using standard specimens

Table 3 shows the mechanical properties of BM and WM obtained using standard tensile and fracture specimens. The tensile parameters shown in the table are the elastic modulus, E, the yield strength, σ_{ys}, the ultimate tensile strength, σ_{ut}, and the tensile elongation, e. The mechanical properties of the HAZ subzones were not determined due to the impossibility of machining homogeneous specimens with the dimensions required by the standards [25,26]. Table 3 also shows the fracture toughness values, determined by means of pre-cracked SENB specimens using the test procedure described in the ASTM E-1820 standard [26]. In the case of BM, the calculated fracture toughness value was J_{IC}, due to its ductile fracture behaviour. WM had brittle behaviour in the same test, so the calculated toughness value was K_{IC} However, J_{IC} is listed in the table based on the existing correlation between these two parameters, assuming a Poisson coefficient, ν, of 0.30.

Table 3. Mechanical properties (mean ± coeff. of variation, %)

Zone	E (GPa)	σ_{ys} (MPa)	σ_{ut} (MPa)	e (%)	J_{IC} (kJ/m^2)
WM	220 ± 9.6	1019 ± 2.1	1120 ± 1.0	16.9 ± 1.2	22 ± 8.1*
BM	209 ± 1.0	597 ± 3.2	710 ± 2.3	18.7 ± 9.1	622 ± 4.5

*Calculated using $J = K_I(1 - \nu^2)/E$

2.3 Small Punch Test characterization

In order to characterize separately the different characteristic zones of the welded joint, BM, CG-HAZ, FG-HAZ and WM, 0.5 mm thickness thin slabs were firstly extracted from the welded coupon. Figure 3.a, shows a macrographic view of the welded coupon and figure 3.b. the schematic position of the extracted slabs. Once it was verified that the microstructure of the slab was correct for the area subject to analysis (BM, CG-HAZ, FG-HAZ and WM), SPT specimens of dimension 10x10x0.5 mm^3 were machined from each slab.

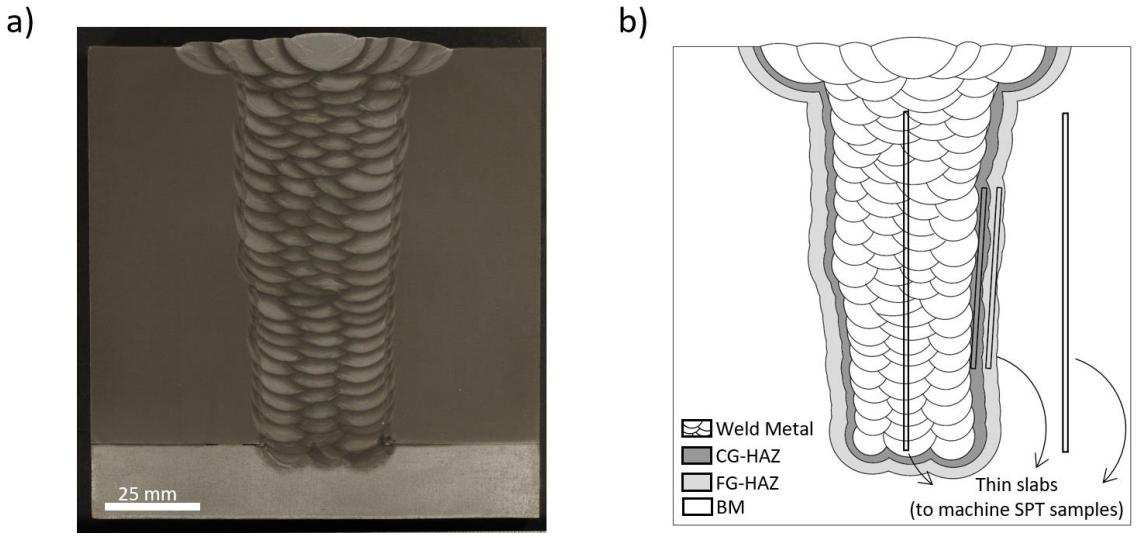

Figure 3. Welded joint. a) Macrography of the welded joint; b) Schematic view of the weld with the different subzones and location of the thin slabs used for SPT characterization

SPTs were carried out using the testing device shown in Figure 4.a mounted in an electromechanical testing machine equipped with a 5 kN load cell and using a COD extensometer to measure the punch displacement. The SPT device has a hemispherical punch with a diameter of 2.5 mm and a lower die with a 4 mm central hole provided by a chamfer with a radius of 0.2 mm. The punch displacement rate was 0.2 mm/min [23,27] and the tests were performed at laboratory ambient conditions.

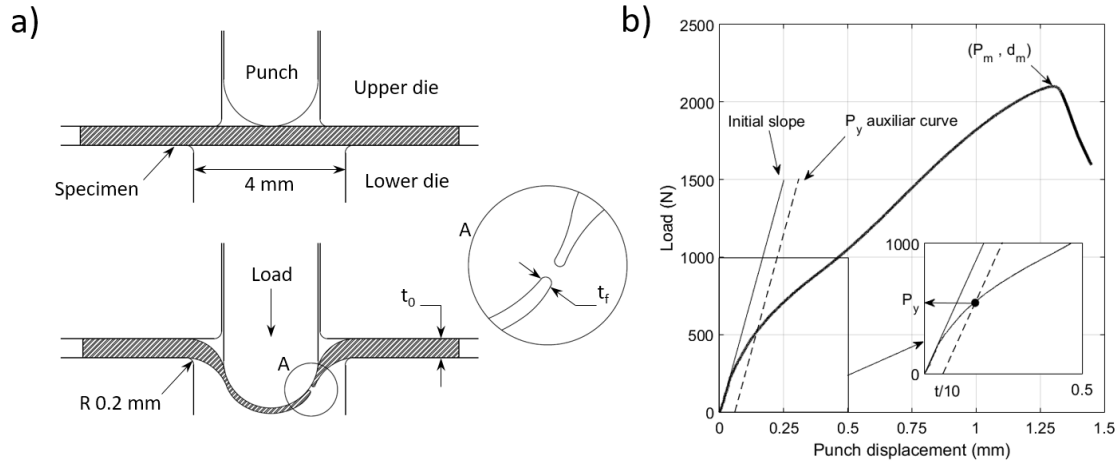

Figure 4. SPT test, a) standard device and biaxial fracture strain determination, ε_{qf}; b) SPT load-displacement plot and calculation of SPT parameters.

Using the conventional SPT samples (without notch), the yield stress, the ultimate tensile strength and the fracture toughness of the different regions of the welded joint are obtained using the equations (1), (2) and (3) respectively. These equations were proposed by T.E. García et al. [1] after characterizing a large number of metallic materials using the same devices and testing procedures.

$$\sigma_{ys} = 0.346 \cdot \frac{P_y}{t^2} \tag{1}$$

$$\sigma_{ut} = 0.277 \cdot \frac{P_m}{d_m \cdot t} \tag{2}$$

$$J_{IC}\left(\frac{kJ}{m^2}\right) = 1695\varepsilon_{qf} - 1320 \tag{3}$$

In these equations, P_y is the load determined from the SPT load-punch displacement curve using the *t/10* offset criterion (Figure 4.b), *t* is the sample thickness, P_m is the maximum load value and d_m is the punch displacement corresponding to this maximum load. As seen in Figure 4.a) .ε_{qf} is the biaxial fracture strain, obtained from equation (4) as the relation between the initial, *t,* and the final, t_f, values of the specimen thickness.

$$\varepsilon_{qf} = ln\left(\frac{t}{t_f}\right) \tag{4}$$

Figure 5 shows the load-displacement SPT curves obtained with the different microstructures. The behaviour of the different regions of the welded joint vary greatly. Although the WM and the CG-HAZ have similar behaviours, the FG-HAZ and especially the BM have much lower curves. From these curves the main SPT parameters were calculated, and they are shown in Table 4 with the estimated tensile and fracture parameters using equations (1), (2) and (3).

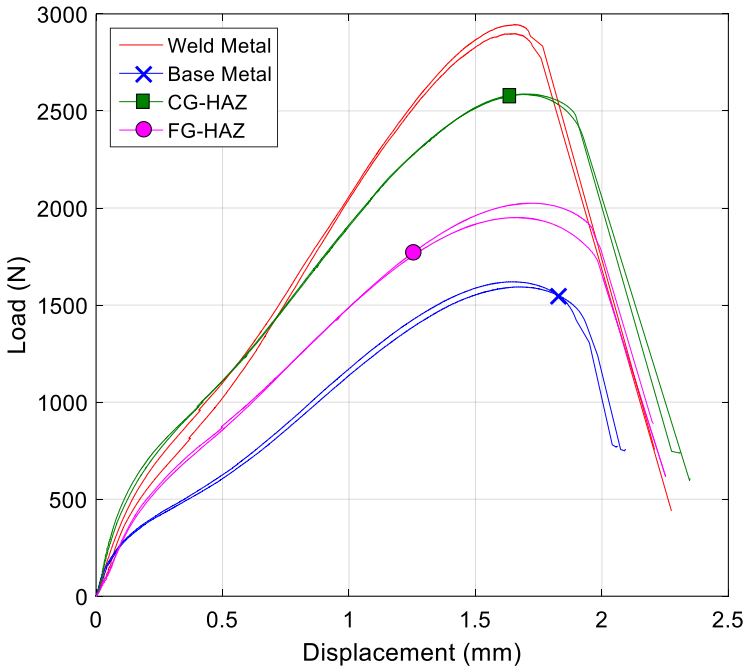

Figure 5. SPT curves of the different weld zones

Table 4. Mechanical properties obtained from the SPT (mean ± Coeff. of variation, %)

Material	P_y/t^2 (MPa)	$P_m/(t \cdot d_m)$ (MPa)	ε_{qf} (-)	σ_{ys} (MPa) Exp. (1)	σ_{ut} (MPa) Exp. (2)	J_{IC} (kJ/m^2) Exp. (3)
WM	2656 ± 12	3603 ± 11	0.7 ± 9	957	1026	<40
CG-HAZ	2133 ± 3	2903 ± 3	0.8 ± 1	738	804	<40
FG-HAZ	1872 ± 4	2166 ± 34	1.1 ± 1	647	600	629
BM	1716 ± 8	2353 ± 23	1.2 ± 1	594	652	731

The tensile and fracture parameters obtained using standard specimens (tensile tests and fracture toughness tests) and SPT samples are compared in Figure 6. As can be seen, regardless of the type of test used, all the results of the tensile properties are similar. Also the fracture toughness of the BM, which had ductile behaviour, was accurately predicted by means of the SPT. Moreover, SPT always gave conservative values of the parameters, providing the confidence necessary for current methodologies.

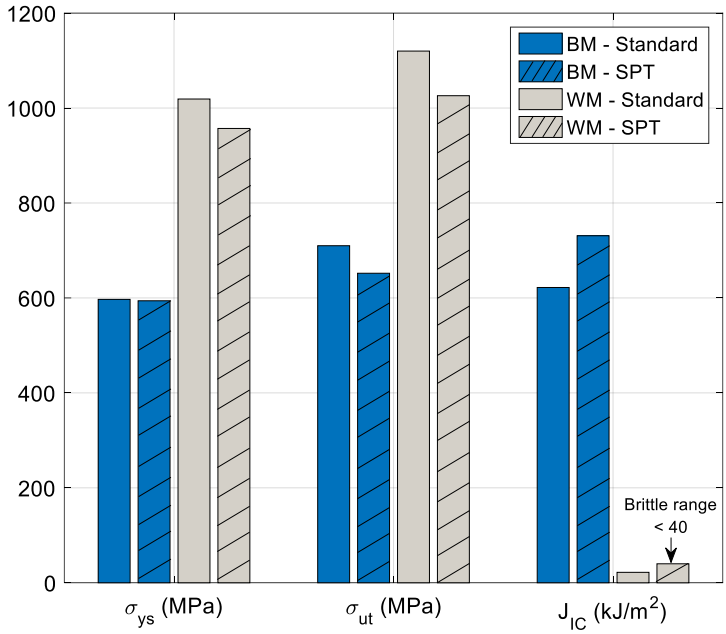

Figure 6. Comparison of mechanical properties using standard specimens and SPT samples

Thus, the use of equations (1) to (3) to calculate the mechanical properties of the different subzones of welds by means of SPT is validated, as well as the values of the HAZ properties shown in Table 4. The table shows that the yield stress and the ultimate tensile strength decrease from the WM to the BM. As SPT samples from the FG-HAZ were extracted from locations very close to the BM (see Figure 3), the mechanical properties of these two regions are nearly equivalent. On the other hand, the yield strength and tensile strength of CG-HAZ is much higher, while the fracture toughness of the GG-HAZ and WM could not be determined using eq. (3), as they have brittle behaviour in the SPT tests. In this case, this equation can only identify the brittle behaviour of the region but not the value of its fracture toughness.

3 Hydrogen embrittlement analysis

3.1 Hydrogen permeation test and precharging procedure

For a better understanding of the influence of hydrogen on the different welded joint microstructures, the effective hydrogen diffusion coefficient, D_{eff}, was determined by means of hydrogen permeation experiments [28–31]. Permeation tests were performed at ambient temperature using a double electrolytic cell, Figure 7.a. The hydrogen permeation specimens had a diameter of 20 mm and a thickness of 1 mm. The specimens were plated on one side with palladium (Pd) to enhance hydrogen oxidation at the hydrogen exit cell of the experiment.

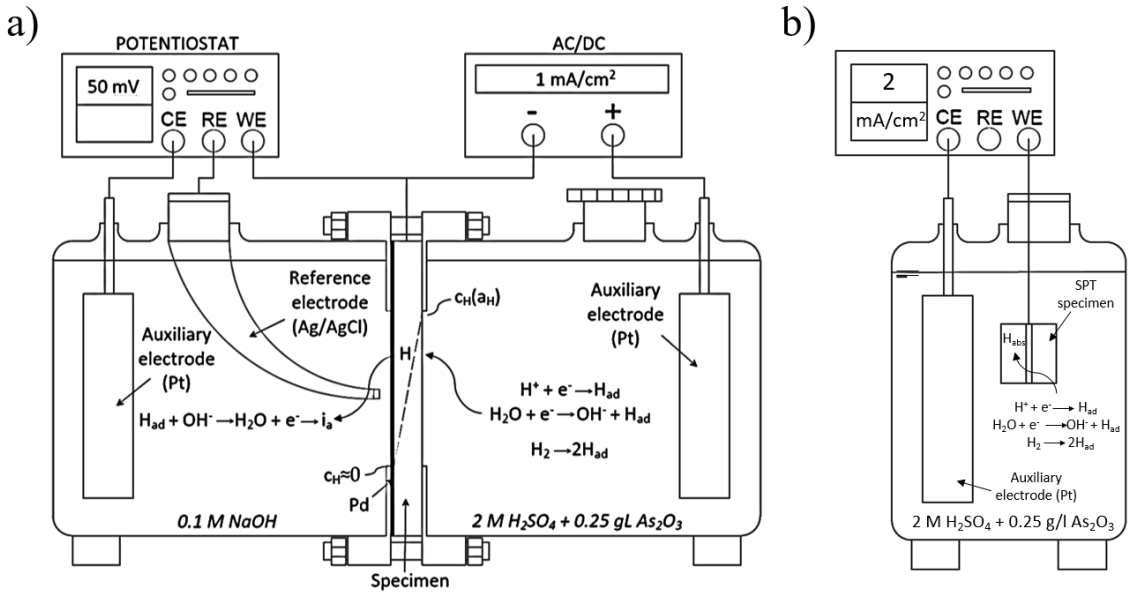

Figure 7. a) Hydrogen permeation cell. b) Cathodic pre-charge

The hydrogen permeation setup is composed of two separate charging and oxidation cells, a reference electrode (Ag/AgCl or SSC), two auxiliary Pt electrodes, and a potentiostat (Figure 7.a). The specimen, with an exposed surface area of 1 cm^2, was mounted between the two cells. The charging cell was galvanostatically polarized at a constant charging current density of 1 $mA \cdot cm^{-2}$ in 2M H_2SO_4 solution with 0.25 g/l As_2O_3 (to avoid hydrogen recombination). On the detection (or oxidation) side of the double cell, the sample was potentiostatically maintained at a constant potential of 50 mV versus a SSC reference electrode in a 0.1M NaOH solution.

The evolution of the anodic current density over time until reaching a steady-state value, i_∞ ($\mu A \cdot m^{-2}$), was measured to determine the diffusion coefficient, D_{eff} (m^2/s), using the

time lag method (Equation 5) derived from Fick's second law, according to the ASTM G148 standard [32].

$$D_{eff} = \frac{d^2}{6t_{0.63}} \tag{5}$$

In the above equation, F (96485 C·mol^{-1}) is the Faraday's constant, d (m) is the specimen thickness, and $t_{0.63}$ (s) is the lag time, defined as the elapsed time at $i/i_{max} = 0.63$.

Figure 8 shows the characteristic permeation curves obtained for the WM, HAZ and BM. The HAZ sample was machined in the middle of the HAZ zone. In this case, the final thickness of the sample was 0.7 mm and the material was a mixture of CG-HAZ and FG-HAZ (checked by means of hardness tests). The permeation results in Table 5 show a decrease of the hydrogen diffusion coefficient from BM to WM, with corresponding values of the HAZ close to those of the WM.

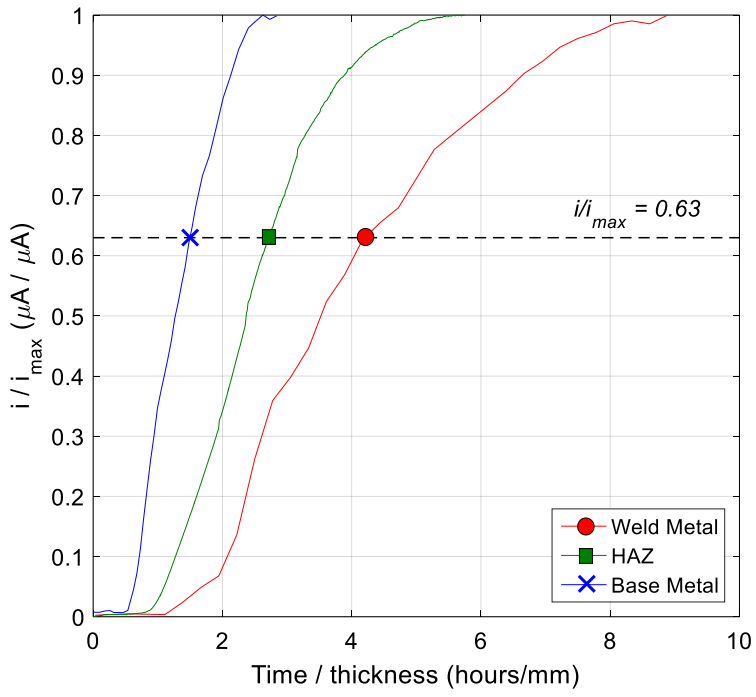

Figure 8. Hydrogen permeation curves

In order to pre-charge the SPT samples with hydrogen, a cathodic precharging method was used. A current density of 2 mA/cm^2 was applied for 4 hours at 20°C [33] using the same electrolyte employed in the charging cell of the double permeation cell, as shown in Figure 7.b.

The quantity of hydrogen introduced in the SPT specimens (C_{H0}) using these precharging conditions was measured using a LECO DH603 analyser. Samples measuring 50 mm in length, 10 mm in width and 1 mm in thickness of MB and WM were pre-charged using the same conditions as the SPT specimens. Also, in order to follow the evolution of the hydrogen concentration with time exposition at laboratory ambient conditions, some of these samples were exposed at the laboratory ambient conditions for 1 month to obtain the residual or strongly trapped hydrogen concentration (C_{HF}). Finally, the diffusible hydrogen was calculated as the difference between the initial and the residual hydrogen concentrations ($C_{Hdiff} = C_{H0} - C_{HF}$). Table 5 shows the results obtained in these tests on BM and WM. Higher initial and diffusible hydrogen concentrations were measured in WM than in BM.

Table 5. Hydrogen permeation and charging results

Material	D_{eff} *(x10^{-11} m^2/s)*	$C_{H0}\ (ppm)$	$C_{HF}\ (ppm)$	$C_{Hdiff}\ (ppm)$
WM	1.1	5.2 ± 0.3	1.1 ± 0.1	4.2 ± 0.3
HAZ	1.4	-	-	-
BM	4.4	4.3 ± 0.5	1.1 ± 0.1	3.2 ± 0.5

3.2 Hydrogen embrittlement analysis with notched pre-charged SPT specimens

As standard SPT specimens are not able to detect hydrogen embrittlement due to their low triaxiality [6], notched SPT samples were used to evaluate this phenomenon by applying an energy criterion . As can be seen in Figure 9, from the middle of a border to the opposite one, a longitudinal no-through-thickness notch with a depth $a = 0.3t$ (t is the specimen thickness) was machined, and the energy at failure, W (Figure 9.b),was determined as the area below the load-displacement curve until the maximum load.

The hydrogen embrittlement analysis was performed using an "Hydrogen Embrittlement Index" (HEI) defined in equation (6), which compares the normalized failure energy obtained testing SPT hydrogen pre-charged specimens (W_H/t^2) with the non-pre-charged (W/t^2) ones.

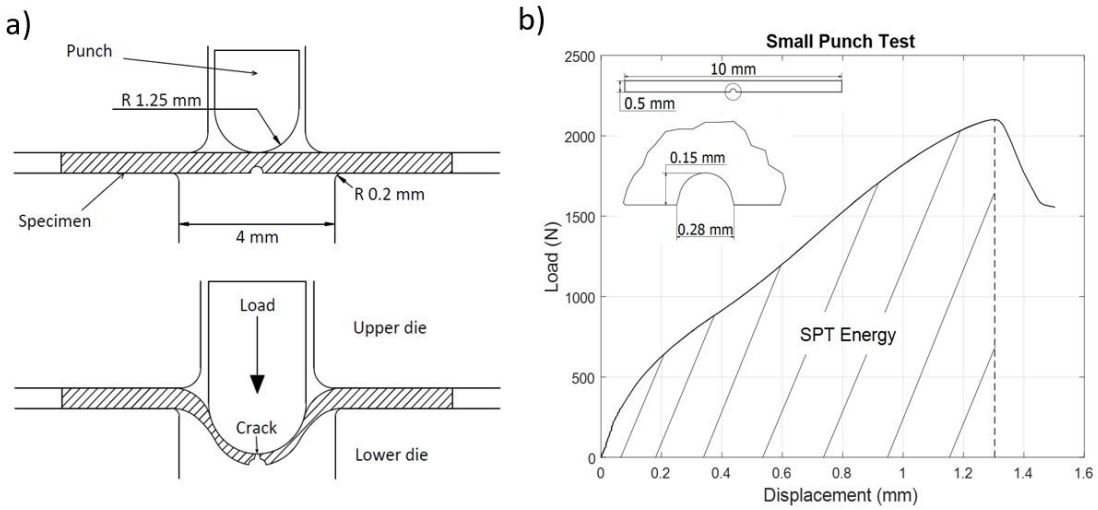

Figure 9. SPT test. a) SPT device; b) SPT curve and geometry for notched samples.

$$HEI\ (\%) = \frac{W/t^2 - W_H/t^2}{W/t^2} \cdot 100 \qquad (6)$$

Figure 10 shows the load-displacement curves obtained after testing the different weld zones. The effect of hydrogen on BM and FG-HAZ was minimal, the shape of the load-displacement curve was not modified, but only a small decrease of the maximum load was apparent. On the other hand, a strong effect of hydrogen was observed on CG-HAZ and WM, where not only a great decrease of the maximum load value has been appreciated, but the shape of the curve has also changed, indicating a change from ductile to brittle behaviour [6].

Table 6 shows the normalized failure energy values obtained in these tests along with their corresponding embrittlement indexes. The embrittlement indexes of BM and FG-HAZ were similar and low, just over 20%. But the hydrogen embrittlement index increases sharply to 63% in the case of CG-HAZ and even higher in the weld metal, WM, exceeding 80%, as these two regions had much higher hardness and strength (see Tables 2 and 4).

These HEI results cannot be directly compared with the results from standard procedures [19] for two reasons: the different hydrogen pre-charging conditions used in each type of test (eloctrolitic pre-charge for SPT vs gaseous pre-charge for standard), and the different

triaxiality exhibited (much lower in the SPT). However, the SPT embrittlement values obtained can be considered valid, since like the standard ones [19,33,34], they show that the phenomenon of hydrogen embrittlement increases with the strength and hardness of the material (see Table 2-3 and 6).

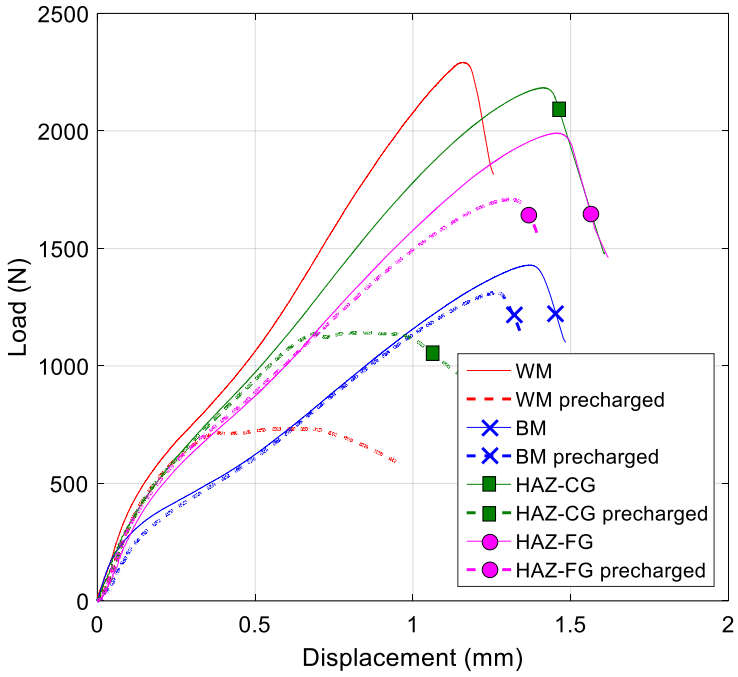

Figure 10. SPT curves of welded joint zones pre-charged with hydrogen

Table 6. Results obtained with notched hydrogen pre-charged SPT samples

Material	W/t^2 *(N/mm)*	W_H/t^2 *(N/mm)*	*HEI (%)*
WM	7140 ± 18	1334 ± 211	81.3
CG-HAZ	6451 ± 481	2389 ± 359	63.0
FG-HAZ	5753 ± 79	4581 ± 311	20.4
BM	5143 ± 61	4032 ± 343	21.6

3.3 Fractographic analysis

The tested SPT samples were observed by means of a scanning electron microscope (SEM JEOL-JSM5600) with an acceleration voltage of 20 kV. The broken samples were previously cleaned for 10 minutes in an acetone bath with ultrasound. Figure 11.a-b shows the failures of hydrogen pre-charged BM and FG-HAZ samples. Both failures were fully ductile, having a fracture appearance similar to the specimens tested without hydrogen: a

single crack initiated at the notch and propagated along the notch, following the maximum stress path.

On the contrary, failure of CG-HAZ and WM specimens were fully brittle, Figure 11.c-d with many radial cracks. Hydrogen diffuses along the test and accumulates in the process zone located ahead of the notch, giving rise to the initiation and propagation of multiple cracks, not only through the specimen thickness ahead of the notch, but also in perpendicular directions.

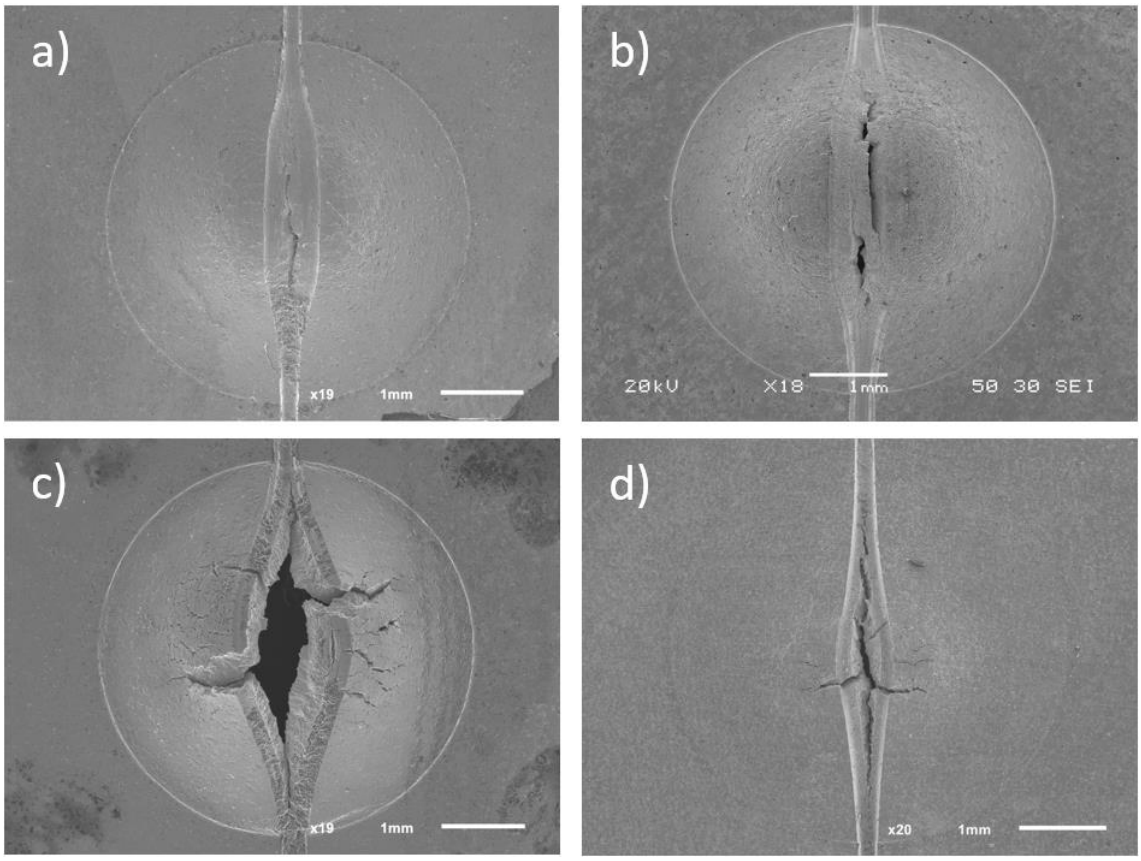

Figure 11. Failed hydrogen pre-charged SPT samples, a) BM; b) FG-HAZ; c) CG-HAZ; d) WM.

4 Conclusions

It was demonstrated that the Small Punch Test allows us to estimate the mechanical properties of small zones, such as the subzones of a weld joint, where the thickness of their particular microstructures is too low to allow machining standard specimens. The

use of equations (1) and (2) was validated to estimate the yield strength and the ultimate tensile strength. Equation (3) also gives good results of the fracture toughness when the behavior of the SPT sample is ductile.

It was not possible to determine the fracture toughness of WM using the standard SPT sample, as its biaxial fracture strain was too low and, in this case, equation (3) was no longer valid. To solve this problem, tests using non-through thickness notched SPT samples were conducted and the normalized energy at failure, W/t^2, was the SPT parameter considered directly related with the fracture toughness. It was seen that the fracture toughness of the FG-HAZ is similar to that of the BM, while the fracture toughness of the CG-HAZ was lower and more similar to that of the WM.

By means of hydrogen permeation experiments, the hydrogen diffusion coefficients of the different microstructures of the weld were determined: a decrease in the hydrogen diffusion coefficient from BM to WM was observed, with corresponding values of the HAZ similar to those of the WM.

Notched SPT specimens were also used to evaluate the hydrogen embrittlement indexes of the different subzones of the CrMoV weld. The effect of hydrogen on the BM and FG-HAZ was low (HEI about 20%) but a strong effect of hydrogen was observed on the CG-HAZ and WM (HEI = 60-80%), where a change from ductile to brittle behaviour was evident. In these latter cases, hydrogen diffuses throughout the test and accumulates in the process zone located ahead of the notch, giving rise to the initiation and propagation of multiple cracks, not only through the specimen thickness ahead of the notch, but also in perpendicular directions.

Rather than carrying out a greater number of tests, with other materials and hydrogen pre-charge conditions, the SPT test using notched specimens and electrolytic pre-charge, seems to be a valid method in the analysis of the hydrogen embrittlement phenomenon for structural steels. Taking into account that the method is able to characterize any area of a structure, no matter how small, and it is also simple and economical, this characterization procedure is presented as an accurate alternative in the experimental study of hydrogen embrittlement in steels.

Acknowledgments

The authors would like to acknowledge the Spanish Ministry of Economy and Competitiveness and the Principality of Asturias government for the financing support given to the RTI2018-096070-B-C31 and IDI/2018/000134 projects, respectively. G. Álvarez (PA-20-PF-BP19-087) and A. Zafra (PA-18-PF-BP17-038) would also thank the Principality of Asturias for the financial support through the Severo Ochoa Scholarship Programme. Authors also thank the financial support received from the Principado de Asturias government through the FC-GRUPIN-IDI/2018/000134 project. Finally, the authors thank the Scientific and Technical Service, University of Oviedo, for the use of the SEM JEOL-JSM5600 scanning electron microscope.

References

[1] T.E. García, C. Rodríguez, F.J. Belzunce, C. Suárez, Estimation of the mechanical properties of metallic materials by means of the small punch test, J. Alloys Compd. 582 (2014) 708–717. doi:10.1016/J.JALLCOM.2013.08.009.

[2] P.M. Bravo Díez, M. Preciado Calzada, D. Cárdenas Gonzalo, J. Calaf Chica, Change of mechanical properties of AM60B alloy with heat treatments and its correlation with small punch tests, Theor. Appl. Fract. Mech. 86 (2016) 101–108. doi:10.1016/J.TAFMEC.2016.09.014.

[3] J. Calaf Chica, P.M. Bravo Díez, M. Preciado Calzada, Development of an improved prediction method for the yield strength of steel alloys in the Small Punch Test, Mater. Des. 148 (2018) 153–166. doi:10.1016/J.MATDES.2018.03.064.

[4] S. Tenneti, P.V. Durgaprasad, N. Naveen Kumar, S.K. Bonagani, J. Chattopadhyay, I. Samajdar, V. Kain, Detection of embrittlement in low alloy steels due to thermal aging by small punch test, Mater. Sci. Eng. A. 759 (2019) 181–194. doi:10.1016/J.MSEA.2019.05.009.

[5] T.E. García, B. Arroyo, C. Rodríguez, F.J. Belzunce, J.A. Álvarez, Small punch test methodologies for the analysis of the hydrogen embrittlement of structural steels, Theor. Appl. Fract. Mech. 86 (2016) 89–100. doi:10.1016/J.TAFMEC.2016.09.005.

[6] T.E. García, C. Rodríguez, F.J. Belzunce, I. Peñuelas, B. Arroyo, Development of a methodology to study the hydrogen embrittlement of steels by means of the small punch test, Mater. Sci. Eng. A. 626 (2015) 342–351. doi:10.1016/j.msea.2014.12.083.

[7] B. Arroyo, J.A. Álvarez, R. Lacalle, C. Uribe, T.E. García, C. Rodríguez, Analysis of key factors of hydrogen environmental assisted cracking evaluation by small

punch test on medium and high strength steels, Mater. Sci. Eng. A. 691 (2017) 180–194. doi:10.1016/J.MSEA.2017.03.006.

[8] P. Dymáček, Recent developments in small punch testing: Applications at elevated temperatures, Theor. Appl. Fract. Mech. 86 (2016) 25–33. doi:10.1016/J.TAFMEC.2016.09.013.

[9] T.E. García, C. Rodríguez, F.J. Belzunce, C. Suárez, Estimation of the mechanical properties of metallic materials by means of the small punch test, J. Alloys Compd. 582 (2014) 708–717. doi:10.1016/j.jallcom.2013.08.009.

[10] J.M. Alegre, R. Lacalle, I.I. Cuesta, J.A. Álvarez, Different methodologies to obtain the fracture properties of metallic materials using pre-notched small punch test specimens, Theor. Appl. Fract. Mech. 86 (2016) 11–18. doi:10.1016/J.TAFMEC.2016.09.006.

[11] I.I. Cuesta, C. Rodriquez, F.J. Belzunce, J.M. Alegre, Analysis of different techniques for obtaining pre-cracked/notched small punch test specimens, Eng. Fail. Anal. 18 (2011) 2282–2287. doi:10.1016/j.engfailanal.2011.08.004.

[12] G. Álvarez, C. Rodríguez, F.J. Belzunce, T.E. García, Use of notched small punch test specimens for the determination of fracture properties in structural steels, Theor. Appl. Fract. Mech. 106 (2020). doi:10.1016/j.tafmec.2019.102442.

[13] T.E. García, C. Rodríguez, F.J. Belzunce, I.I. Cuesta, Development of a new methodology for estimating the CTOD of structural steels using the small punch test, Eng. Fail. Anal. 50 (2015) 88–99. doi:10.1016/j.engfailanal.2015.01.011.

[14] E. Martínez-Pañeda, I.I. Cuesta, I. Peñuelas, A. Díaz, J.M. Alegre, Damage modeling in Small Punch Test specimens, Theor. Appl. Fract. Mech. 86 (2016) 51–60. doi:10.1016/J.TAFMEC.2016.09.002.

[15] A.H.S. Bueno, E.D. Moreira, J.A.C.P. Gomes, Evaluation of stress corrosion cracking and hydrogen embrittlement in an API grade steel, Eng. Fail. Anal. 36 (2014) 423–431. doi:10.1016/J.ENGFAILANAL.2013.11.012.

[16] A. Zafra, L.B. Peral, J. Belzunce, C. Rodríguez, Effect of hydrogen on the tensile properties of 42CrMo4 steel quenched and tempered at different temperatures, Int. J. Hydrogen Energy. (2018). doi:10.1016/j.ijhydene.2018.03.158.

[17] X. Li, J. Zhang, S. Shen, Y. Wang, X. Song, Effect of tempering temperature and inclusions on hydrogen-assisted fracture behaviors of a low alloy steel, Mater. Sci. Eng. A. 682 (2017) 359–369. doi:10.1016/j.msea.2016.11.064.

[18] J. Moon, J. Choi, S.-K. Han, S. Huh, S.-J. Kim, C.-H. Lee, T.-H. Lee, Influence of precipitation behavior on mechanical properties and hydrogen induced cracking during tempering of hot-rolled API steel for tubing, Mater. Sci. Eng. A. 652 (2016) 120–126. doi:10.1016/J.MSEA.2015.11.083.

[19] L.B. Peral, A. Zafra, J. Belzunce, C. Rodríguez, Effects of hydrogen on the fracture toughness of CrMo and CrMoV steels quenched and tempered at different temperatures, Int. J. Hydrogen Energy. 44 (2019) 3953–3965. doi:10.1016/J.IJHYDENE.2018.12.084.

[20] G. Álvarez, L.B. Peral, C. Rodríguez, T.E. García, F.J. Belzunce, Hydrogen embrittlement of structural steels: Effect of the displacement rate on the fracture

toughness of high-pressure hydrogen pre-charged samples, Int. J. Hydrogen Energy. (2019). doi:10.1016/j.ijhydene.2019.03.279.

[21] A. Zafra, L.B. Peral, J. Belzunce, C. Rodríguez, Effects of hydrogen on the fracture toughness of 42CrMo4 steel quenched and tempered at different temperatures, Int. J. Press. Vessel. Pip. 171 (2019) 34–50. doi:10.1016/J.IJPVP.2019.01.020.

[22] M.B. Djukic, V. Sijacki Zeravcic, G.M. Bakic, A. Sedmak, B. Rajicic, Hydrogen damage of steels: A case study and hydrogen embrittlement model, Eng. Fail. Anal. 58 (2015) 485–498. doi:10.1016/J.ENGFAILANAL.2015.05.017.

[23] C. Rodríguez, J. García Cabezas, E. Cárdenas, F.J. Belzunce, C. Betegón, Mechanical properties characterization of heat-affected zone using the small punch test, Weld. J. (Miami, Fla). 88 (2009) 188s-192s. http://www.scopus.com/inward/record.url?eid=2-s2.0-70349446383&partnerID=40&md5=61c83bc5932eddaaa242faa6b225a2d4.

[24] C. Rodríguez, E. Cárdenas, F.J. Belzunce, C. Betegón, Fracture Characterization of Steels by Means of the Small Punch Test, Exp. Mech. 53 (2013) 385–392. doi:10.1007/s11340-012-9637-x.

[25] U.-E.I. 6892-1, Materiales metálicos Ensayo de tracción Parte 1 : Método de ensayo a temperatura ambiente, (2017).

[26] ASTM E 1820-01: Standard Test Method for Measurement of Fracture Toughness, 2001. doi:10.1520/E1820-09.2.

[27] T.E. García, C. Rodríguez, F.J. Belzunce, C. Suárez, Estimation of the mechanical properties of metallic materials by means of the small punch test, J. Alloys Compd. 582 (2014) 708–717. doi:10.1016/J.JALLCOM.2013.08.009.

[28] P. Castaño Rivera, V.P. Ramunni, P. Bruzzoni, Hydrogen trapping in an API 5L X60 steel, Corros. Sci. 54 (2012) 106–118. doi:10.1016/J.CORSCI.2011.09.008.

[29] Q. Liu, A. Atrens, Reversible hydrogen trapping in a 3.5NiCrMoV medium strength steel, Corros. Sci. 96 (2015) 112–120. doi:10.1016/J.CORSCI.2015.04.011.

[30] T. Zhang, W. Zhao, T. Li, Y. Zhao, Q. Deng, Y. Wang, W. Jiang, Comparison of hydrogen embrittlement susceptibility of three cathodic protected subsea pipeline steels from a point of view of hydrogen permeation, Corros. Sci. 131 (2018) 104–115. doi:10.1016/J.CORSCI.2017.11.013.

[31] W. Zhao, T. Zhang, Y. Zhao, J. Sun, Y. Wang, Hydrogen permeation and embrittlement susceptibility of X80 welded joint under high-pressure coal gas environment, Corros. Sci. 111 (2016) 84–97. doi:10.1016/J.CORSCI.2016.04.029.

[32] ASTM Standard G148 - 1997, Standard practice for evaluation of hydrogen uptake, permeation and transport in metals by an electrochemical technique, i (1997) 10. doi:10.1520/G0148-97R11.2.

[33] G. Álvarez, A. Zafra, F.J. Belzunce, C. Rodríguez, Hydrogen embrittlement analysis in a CrMoV steel by means of sent specimens, Theor. Appl. Fract. Mech. 106 (2020). doi:10.1016/j.tafmec.2019.102450.